Journal of Solid State Chemistry 184 (2011) 3050–3054

Contents lists available at SciVerse ScienceDirect

Journal of Solid State Chemistry

journal homepage: www.elsevier.com/locate/jssc

Synthesis of large surface area nano-sized $BiVO_4$ by an EDTA-modified hydrothermal process and its enhanced visible photocatalytic activity

Wanting Sun, Mingzheng Xie, Liqiang Jing*, Yunbo Luan, Honggang Fu*

Key Laboratory of Functional Inorganic Materials Chemistry (Heilongjiang University), Ministry of Education, School of Chemistry and Materials Science, Harbin 150080, PR China

ARTICLE INFO

Article history:
Received 16 April 2011
Received in revised form
8 September 2011
Accepted 14 September 2011
Available online 17 September 2011

Keywords:
$BiVO_4$
Hydrothermal process
EDTA chelation
Large surface area
Visible photocatalysis

ABSTRACT

In this work, monoclinic scheelite-type $BiVO_4$ nanoparticle with large surface area has been successfully synthesized, using $Bi(NO_3)_3$ and NH_4VO_3 as raw materials, through a hydrothermal process in the presence of ethylene diamine tetraacetic acid (EDTA). It is demonstrated that the nanoparticle size of as-prepared $BiVO_4$ becomes small by decreasing hydrothermal temperature, shortening hydrothermal reaction time and increasing EDTA amount used. The resulting $BiVO_4$ nanoparticle with large surface area exhibits a good photocatalytic performance for degrading phenol solution as a model organic pollutant under visible illumination. The key of this method is the chelating role of EDTA group in the synthetic process that it can greatly control the concentration of Bi^{3+}, leading to the growth inhibition of $BiVO_4$ crystallite. The work provides a route for the synthesis of Bi-containing nano-sized composite oxides with large surface area.

1. Introduction

Bismuth vanadate, well-known for applications in pigments [1], ionic conductivity [2], and ferroelasticity [3], has recently attracted extensive attentions for using in water splitting and organic contaminant decomposition as a result of its visible-light-driven photochemical properties [4–9]. Kudo et al. found that $BiVO_4$ absorbs well visible spectrum and has the capacity for O_2 evolution from $AgNO_3$ solutions [6–8]. And Li et al. demonstrated that $BiVO_4$ nanosheets have the ability to degrade *N*,*N*,*N*′,*N*′-tetraethylated rhodamine (RB) under visible-light illumination [10].

Monoclinic scheelite $BiVO_4$ with high photocatalytic activity among its three crystalline phases [11] has been prepared by various methods, such as solid-state reaction method [12–14], aqueous process [15,16], hydrothermal process [17,18], and chemical bath deposition [19]. Generally, nanoparticle size and surface area of the photocatalyst could intensely influence its activity [20,21]. However, the $BiVO_4$ particle synthesized by the techniques mentioned above usually has a large average diameter, leading to a small surface area spontaneously. This is mainly due to the high calcination temperature required often in the solid-state reaction, and to the tiny solubility product of $BiVO_4$ in itself in the aqueous synthetic reactions. Generally speaking, small surface area may strongly limit photocatalytic activity of $BiVO_4$. Given this situation, it is of great significance to develop a method to synthesize nano-sized $BiVO_4$ with large surface area for its further practical application.

There have been several reports that $BiVO_4$ with small nanoparticle size and large surface area were obtained by metalorganic decomposition [22]. However, the exorbitant price of the organic bismuth and vanadium and the complex synthetic process make the method unfit to widespread application. Hence, it is enthusiastic expected to develop a method characterized as simple process and low cost to prepare nano-sized $BiVO_4$ using inorganic bismuth and vanadium as raw materials.

After the analysis of aqueous process, it is considered that the large size of $BiVO_4$ particle prepared is attributed to the tiny solubility product of $BiVO_4$ in the aqueous solution [23], which leads to its rapid nucleation and crystallite growth. In view of this situation, to reduce the concentration of the reactant may be an effective way to control the growth of $BiVO_4$ crystallite. Choosing a suitable chelating agent to react with the reactant is an expected method to reduce its concentration. Widely accepted, EDTA is a classical chelating agent and often used in the analysis as a kind of masking agents. It is characterized by carboxyl groups at either end of the molecule and has six coordination atoms interacting with metal ions in the solution to form coordination complexes. Thus, if the EDTA is introduced into the aqueous synthetic process, it would react with reactant ions to form chelate complexes, and then gradually release metallic ions under certain conditions. Hopefully, the concentration of the reactant would be controlled in a very low level so that the growth of $BiVO_4$ crystallite would be obviously inhibited accordingly. Recently, Sun et al. reported that nanoplate-stacked star-like

* Corresponding authors. Fax: +86 451 86673647.
E-mail address: Jinglq@hlju.edu.cn (L. Jing).

0022-4596/$ - see front matter © 2011 Elsevier Inc. All rights reserved.
doi:10.1016/j.jssc.2011.09.013

$BiVO_4$ products had been synthesized by a hydrothermal method in the presence of EDTA [24], and it was demonstrated that the EDTA played an important role in determining the $BiVO_4$ morphology. Unfortunately, the diameter of the $BiVO_4$ particle obtained exceeds 2 μm, leading to a small surface area. The main cause, we consider, is that the EDTA does not react with reactant ions to reduce their concentration since low reactant concentration is beneficial to inhibit the growth of crystallite, in other words, the $BiVO_4$ particles produced in the precipitation process is rather large prior to the hydrothermal process.

In this paper, we have developed an EDTA-modified hydrothermal method to synthesize monoclinic scheelite-type nano-$BiVO_4$ particles with large surface area at low hydrothermal temperature. Different from the report [24], EDTA is introduced prior to the precipitation process. In the synthetic process, the EDTA reacts with Bi^{3+} to form stable chelate complex, reducing the Bi^{3+} concentration. Thus, the growth of $BiVO_4$ crystallite is well controlled. Compared to the $BiVO_4$ synthesized by the conventional un-modified hydrothermal process, the as-prepared $BiVO_4$ has a good photocatalytic performance for photochemical degradation of phenol solution under visible light illumination. This work provides a feasible approach to the synthesis of Bi-containing nano-sized composite oxides with large surface area, which is favorable to enhance activity.

2. Experimental section

2.1. Synthesis of materials

All of the reagents are analytical grade and used without further purification. $BiVO_4$ was prepared through an EDTA-modified hydrothermal process. In a typical experiment, 0.01 mol $Bi(NO_3)_3 \cdot 5H_2O$ and desired amount EDTA were dissolved in 100 ml 2 mol/L of HNO_3 solution under vigorous agitation at room temperature. Afterwards, 0.01 mol NH_4VO_3 was added into the above mixture and continuously stirred for 30 min to form a homogeneous solution. Then, the resulting solution was transferred into a Teflon-lined stainless steel autoclave to carry out hydrothermal reactions at a certain temperature. After the autoclave was allowed to cool to the room temperature naturally, the product collected was washed with distilled water and absolute ethanol in turn, and dried at 60 °C in air. At last, the samples obtained are represented by BVO–*X*–*Y*–*Z*, in which BVO means $BiVO_4$, *X* is the molar ratio of EDTA to $Bi(NO_3)_3$, *Y* is the hydrothermal temperature and *Z* is the hydrothermal reaction time.

2.2. Characterizations

The X-ray powder diffraction (XRD) patterns were collected on a Rigaku D/MAX-rA powder diffractometer (Japan), using Cu*K*α radiation (λ=0.15418 nm), and an accelerating voltage of 30 kV and emission current of 20 mA were employed; Transmission electron microscopy (TEM) observation was completed on a JEOL JEM-2010EX instrument operated at 200 kV accelerating voltage; the specific surface areas of the samples were measured by BET instrument (Micromeritics automatic surface area analyzer Gemini 2360, Shimadzu), with nitrogen adsorption at 77 K; the Fourier transform infrared spectra (FT-IR) of the samples were obtained through a Bruker Equinox 55 Spectrometer, using KBr as diluents; the UV–vis diffuse reflectance spectra (DRS) were recorded with a Model Shimadzu UV2550 spectrophotometer; the surface photovoltage spectroscopy (SPS) measurements of samples were carried out with a home-built apparatus that had been described in detail elsewhere [25–27].

2.3. Evaluation of visible photocatalytic activity

Phenol is commonly regarded as a typical recalcitrant and colorless pollutant. Thus, it is chosen as a representative organic substance to evaluate visible photocatalytic activity of the as-prepared $BiVO_4$. The photocatalytic experiments were performed in a 100 ml of open photochemical glass reactor equipped with an optical system provided from a side of the reactor by a 150 W GYZ220 high-pressure Xenon lamp made in China with a cut-off filter ($\lambda > 420$ nm), which was placed at about 10 cm from the reactor. During the evaluation of photocatalytic degradation of phenol, 0.05 g of the $BiVO_4$ sample and 80 ml of 5 mg/L phenol solution were mixed by a magnetic stirrer for 4 h under visible light irradiation. Sample was taken at 1 h intervals and the phenol concentration was analyzed by the colorimetric method of 4-aminoantipyrine after centrifugation with a Model Shimadzu UV2550 spectrophotometer.

3. Results and discussion

3.1. Crystal phase and crystallinity

The X-ray diffraction (XRD) is often used to analyze the crystal structure and crystallization degree of sample, and the crystallite size of sample can also be determined from the broadening of corresponding X-ray spectral peak by Scherrer formula [28]. Fig. 1 shows the XRD patterns of different $BiVO_4$ samples. It is confirmed that the resulting $BiVO_4$ is monoclinic scheelite-type according to the standard cards JCPDS 14-0688. That is to say, the introduction of EDTA does not change the sample's crystal structure. Compared to the un-modified BVO-0-90-6, the XRD diffraction peaks of modified BVO-1-90-6 become weak and wide significantly (Fig. 1A), indicating that it has a small crystallite size. Moreover, it can be seen that, as the hydrothermal temperature increases, the XRD peaks gradually become strong, demonstrating that the sample's crystallinity and corresponding crystallite size increase gradually. When the hydrothermal temperature increases to120 °C, the XRD peaks of the resulting $BiVO_4$ have no obvious difference from those of un-modified BVO-0-90-6, indicating that the EDTA introduced has a weak inhibition effects on the growth of crystallites as the reaction temperature reaches to 120 °C. In addition, when the hydrothermal temperature is lower than 90 °C, there is nearly no $BiVO_4$ production. Thus, it is suggested that the hydrothermal temperature between 90 and 120 °C is proper for EDTA exhibiting an obvious effect on the controllable synthesis of nano-sized $BiVO_4$.

The EDTA concentration is also a crucial effect on the formation of the final $BiVO_4$ nanoparticles. Fig. 1B shows that, as the EDTA concentration increases, the crystallinity and particle size of the resulting $BiVO_4$ decrease, meaning that high EDTA concentration is beneficial to control the growth of nanoparticles. Nonetheless, it is worthwhile to note that, when the EDTA concentration is fixed at 1.5 (the molar ratio of EDTA to $Bi(NO_3)_3$), the resulting sample is amorphous. Expectedly, with prolonging the reaction time, the crystallization degree of $BiVO_4$ sample is increased by means of XRD patterns (Supporting information (SI)-I). Thus, short hydrothermal reaction time is favorable for the small-nanosized $BiVO_4$.

3.2. Morphology and specific surface areas

The TEM photographs of $BiVO_4$ prepared under different conditions are shown in Fig. 2. As shown in Fig. 2A, the BVO-0-90-6 with irregular sphere form has an average diameter of about 100 nm, while the BVO-1-90-6 with a similar sphere form has an average size of approximate 20 nm. As the XRD demonstrating, when the hydrothermal temperature rises to 110 °C (SI-II(A)), the

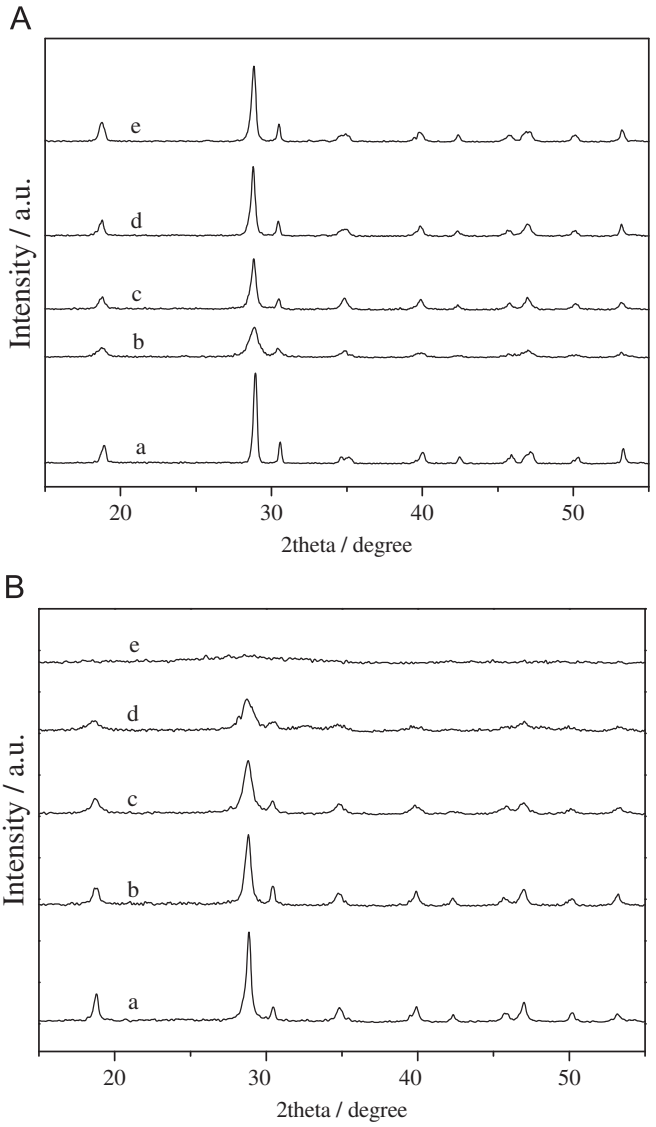

Fig. 1. XRD patterns of different $BiVO_4$ samples: **A.** (a) BVO-0-90-6; (b) BVO-1-90-6; (c) BVO-1-100-6; (d) BVO-1-110-6; (e) BVO-1-120-6. **B.** (a) BVO-0.5-90-6; (b) BVO-0.8-90-6; (c) BVO-1-90-6; (d) BVO-1.3-90-6; (e) BVO-1.5-90-6.

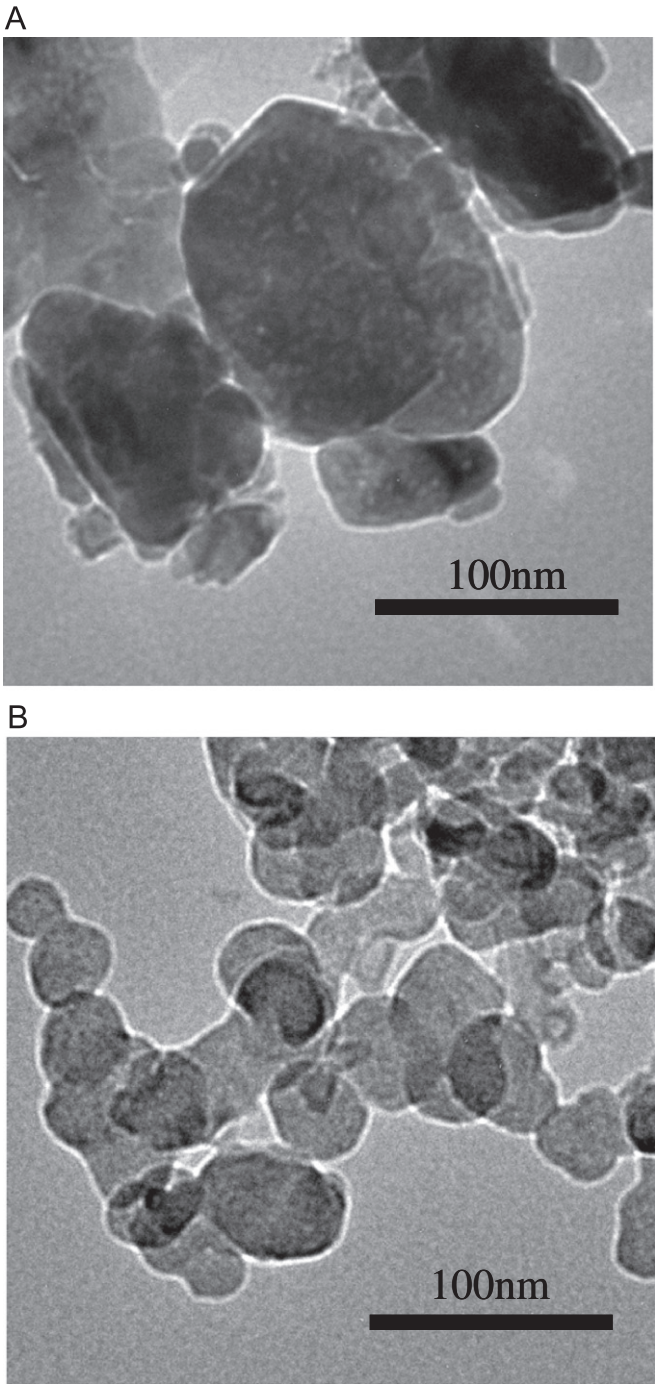

Fig. 2. TEM images of different $BiVO_4$ samples: **A.** BVO-0-90-6 and **B.** BVO-1-90-6.

molar concentration ratio of used EDTA to Bi^{3+} reduces to 0.5 (SI-II(B)), and the hydrothermal reaction time prolongs to 10 h (SI-II(C)), the nanoparticle size of the resulting $BiVO_4$ increases to some extent, about from 30 to 50 nm. Thus, it is concluded that the nanoparticle size of $BiVO_4$ is controllably changed through adjusting the reaction conditions like used EDTA amount, reaction temperature and time. Small nanoparticle size should correspond to large surface area. The BET surface area of BVO-1-90-6 is 10.36 $m^2\ g^{-1}$, which is much larger (over 12 times) than that of BVO-0-90-6 (0.72 $m^2\ g^{-1}$).

3.3. Synthetic mechanism

In the synthesis of $BiVO_4$ by the aqueous-state reaction, $Bi(NO_3)_3$ and NH_4VO_3 are used as material resources. As expected, Bi^{3+} will produce when $Bi(NO_3)_3$ is dissolved in acidic solution, and VO_3^- will produce when NH_4VO_3 is dissolved in water. Then, $BiVO_4$ will produce immediately when the Bi^{3+}-containing and VO_3^--containing solutions are mixed [29]. Widely accepted, $BiVO_4$ will produce with a quick kinetic growth process when high content of free Bi^{3+} and VO_3^- meet, which is responsible for the large particle size of $BiVO_4$ obtained.

However, if the EDTA is introduced into the reactive system, the Bi^{3+} in the acidic solution would react with $EDTA^-$ to form stable chelate complexes via the electrostatic attractions, which greatly decreases the free Bi^{3+} content in the solution, even without free Bi^{3+} in the ambient temperature [30]. Thus, when the NH_4VO_3 is added, the $BiVO_4$ would slowly produce. In the subsequent hydrothermal process, the chelate complexes would be dissociated gradually to provide a small amount of free Bi^{3+}. Since the release rate of Bi^{3+} is rather slow so that its concentration in the solution is very low, leading to a slow kinetic growth process corresponding to the small particle size. With increasing

hydrothermal temperature, the amount of free Bi^{3+} resulting from the dissociation of the chelate complexes would be increased gradually, leading to a little quick kinetic growth process corresponding to a little large particle size. Therefore, the kinetic process of $BiVO_4$ formation could be controlled by changing the used EDTA concentration, reactive temperature and time, further controlling the size of $BiVO_4$ nanoparticle. The above assumption is further supported by the FT-IR spectra. Fig. 3(c) shows that the EDTA has characteristic IR peaks as follows. The absorptions at 3600 and 3200 cm^{-1} are generally attributed to O–H and N–H stretching vibrations [31,32], respectively, and the absorption at 670 cm^{-1} corresponds to the C–N stretching vibration in the strong acidic environment [32]. The absorptions at 1634 and 1365 cm^{-1} are attributed to C=O stretching vibration [33]. When the bismuth ions exist, the principal EDTA absorption peaks at 3600 and 1634 cm^{-1} become weak, even disappear (Fig. 3(d)), manifesting that Bi^{3+} easily reacts with $EDTA^-$ to form a stable Bi^{3+}–EDTA chelate complexes mainly via $-COO^-$ groups. However, the IR absorption peaks of EDTA do not disappear in the presence of VO_3^- (Fig. 3(e)), implying that the VO_3^- hardly reacts with $EDTA^-$. This is attributed to their coulomb repulsion. It is worthwhile to note that the characteristic peaks of the EDTA re-appear after hydrothermal reactions, demonstrating that the EDTA is re-released from the complexes due to the slow formation of $BiVO_4$. Based on the above statement, possible synthetic reaction mechanisms are suggested as follows:

$$Bi(NO_3)_3 \rightarrow Bi^{3+} + 3NO_3^- \quad (1)$$

$$Bi^{3+} + EDTA^- \rightarrow (Bi^{3+} - EDTA)\ \text{chelate compound} \quad (2)$$

$$NH_4VO_3 \rightarrow NH_4^+ + VO_3^- \quad (3)$$

$$(Bi^{3+} - EDTA) + VO_3^- + H_2O \xrightarrow{\text{hydrothermaltreatment}} Bi^{3+} + EDTA^- + VO_3^- + H_2O \rightarrow BiVO_4 + EDTA^- + 2H^+ \quad (4)$$

Since there is a certain amount of EDTA in the reaction system after hydrothermal reactions, nanoplate-stacked-like $BiVO_4$ products should occur according to Ref. [24] if the hydrothermal reaction time is long enough. Interestingly, this is seemingly proved by the TEM image (SI-II(C)) of the $BiVO_4$ sample synthesized by the 10-h hydrothermal reaction.

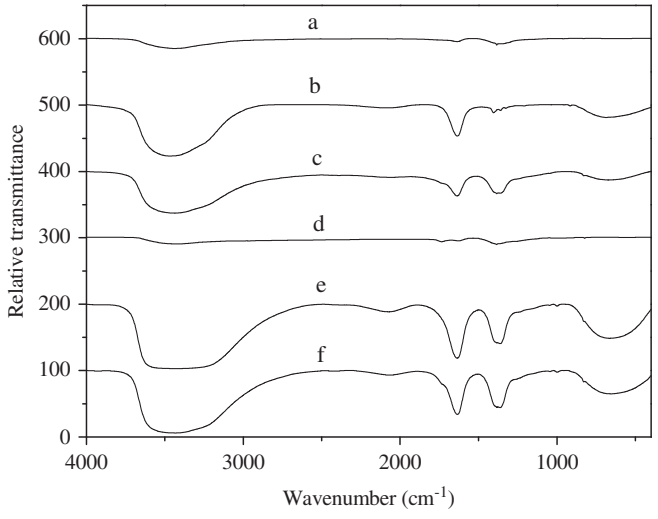

Fig. 3. IR spectra of different samples: (a) HNO_3 solution (2 mol/L); (b) EDTA solution (0.1 mol/L); (c) HNO_3 solution (2 mol/L) containing 0.1 mol/L EDTA; (d) HNO_3 solution (2 mol/L) containing 0.1 mol/L $Bi(NO_3)_3$ and 0.1 mol/L EDTA; (e) HNO_3 solution (2 mol/L) containing 0.1 mol/L NH_4VO_3 and 0.1 mol/L EDTA; (f) reactive solution after hydrothermal process at 90 °C for 6 h.

3.4. Evaluation of visible photocatalytic activity

Phenol is hardly adsorbed on catalysts such as TiO_2 or $BiVO_4$ from its aqueous solution, so its photodegradation is always more difficult than those adsorbable pollutants [34]. It is seen from Fig. 4 that the photocatalytic activity of BVO-0-90-6 is very low, while the as-prepared $BiVO_4$ displays remarkably high activity. And the BVO-1-90-6 exhibits higher activity than the BVO-1-110-6. Noticeably, the photocatalytic degradation of phenol is incomplete on $BiVO_4$, accompanying by main intermediate products (SI-III). Based on the measurement results of XRD, TEM and BET, it is deduced that the enhancement of photocatalytic activity is mainly attributed to the increased surface area resulting from the obvious decrease in the nanoparticle size, which is further supported by the SI-IV, in which one could see that the photocatalytic activity increases as the nanoparticle size decreases over different resulting $BiVO_4$. In addition, for BVO-1-90-6 sample, the relationship between the photocatalytic activity and the used light wavelength (SI-V), and the effects of O_2 concentration on its activity (SI-VI) were investigated. Expectedly, when the wavelength is larger than 500 nm corresponding to the absorption edge of the $BiVO_4$ sample, the sample has almost no photocatalytic activity. As the wavelength decreases continuously, the photocatalytic activity increases gradually. When the wavelength decreases to 400 nm, the sample activity becomes stable basically. It is consistent with the following DRS result. It is confirmed that, with the O_2 concentration increasing, the photocatalytic activity increases gradually, indicating that dissolved oxygen is favorable to promote the photocatalytic degradation of phenol.

Moreover, it is expected that the band gap of the resulting $BiVO_4$ would become wide due to the quantum size effect. Indeed, as the nanoparticle size decreases, the blue shift in the DRS absorption spectra (Fig. 5A) can be seen, and their SPS responses (Fig. 5B) gradually become low. Our previous study indicates that the SPS signal of nano-semiconductor will get weak as the nanoparticle size decreases [25]. Thus, the DRS and SPS results also further demonstrate the change trend in the nanoparticle size.

It is worth noting that, for the DRS and SPS spectra, their response edges are similar, indicating that the conduction band bottom energy level of $BiVO_4$ is high enough that the photoinduced electrons can be captured by the adsorbed oxygen based on the SPS principle. This would lead to its high photoinduced charge separation rate in itself, which makes us clear why $BiVO_4$

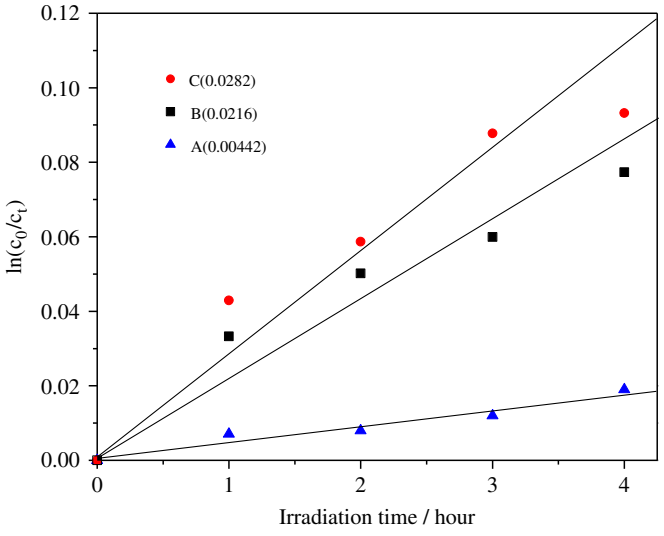

Fig. 4. Photocatalytic evolution curves of phenol solution on (a) BVO-0-90-6; (b) BVO-1–110-6; and (c) BVO-1-90-6.

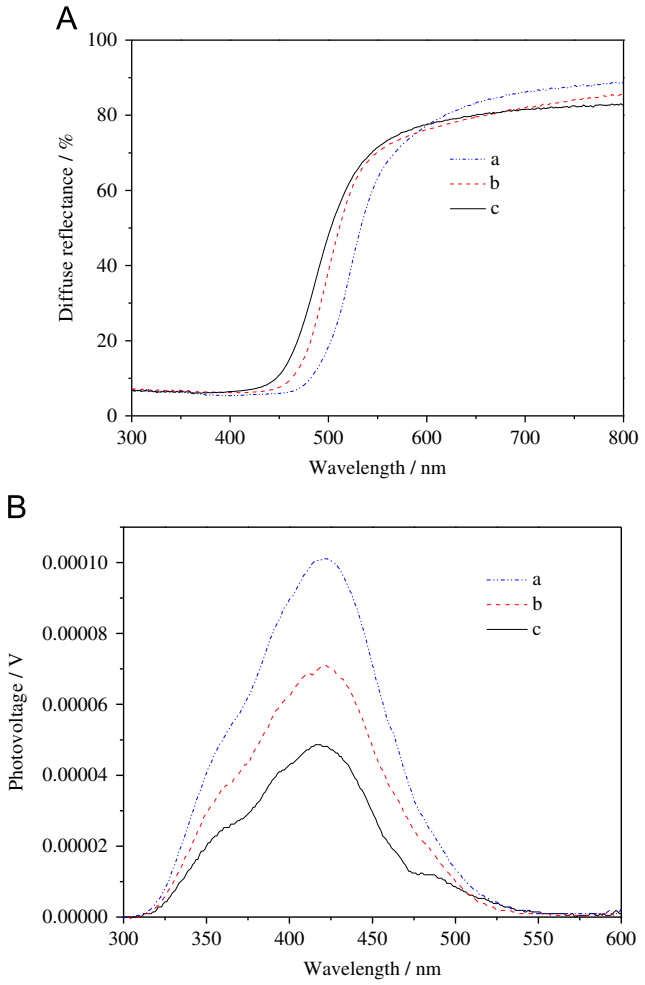

Fig. 5. A. DRS spectra of different $BiVO_4$ samples: (a) BVO-0-90-6; (b) BVO-1-110-6; (c) BVO-1-90-6; **B.** SPS responses of different $BiVO_4$ samples: (a) BVO-0-90-6; (b) BVO-1-110-6; (c) BVO-1-90-6.

always possesses a better photocatalytic performance than other common oxide semiconductors with narrow gap, like Fe_2O_3 and WO_3.

4. Conclusions

In summary, through a hydrothermal process in the presence of ethylene diamine tetraacetic acid (EDTA), monoclinic scheelite-type $BiVO_4$ nanoparticle with large surface area is synthesized successfully. As the hydrothermal temperature reduces, the hydrothermal time shortens, and the EDTA concentration increases, the nanoparticle size of the resulting $BiVO_4$ becomes small. By adjusting the reaction conditions, the $BiVO_4$ samples with an average particle size from 20 to 50 nm can be obtained. Based on the FT-IR spectra, it is confirmed that the introduction of EDTA can coordinate with Bi^{3+} to form a stable Bi^{3+}–EDTA chelate compound, consequently keeping a low-content free Bi^{3+} in the reaction system and then inhibiting the growth of $BiVO_4$ crystallite during the hydrothermal processes. Compared with the conventional chemical precipitation, the as-prepared $BiVO_4$ sample shows a high photocatalytic activity, mainly due to its small particle size and large surface area. The synthetic route provides guidance for the synthesis of Bi-containing nano-sized composite oxides with large surface area using EDTA as an effective modifier.

Supporting information available

XRD patterns, TEM images, main intermediate products, the relationship between particle size and photocatalytic activity, the relationship between the photocatalytic activity and the used light wavelength, and the effects of O_2 concentration on the activity.

Acknowledgment

This work is financially supported from the National Nature Science Foundation of China (No. 21071048), the Science Foundation of Harbin City of China (No. 2011RFXXG001), and the Program for Innovative Research Team in Heilongjiang University (Hdtd2010-02), for which we are very grateful.

Appendix A. Supporting materials

Supplementary data associated with this article can be found in the online version at doi:10.1016/j.jssc.2011.09.013.

References

[1] P. Wood, F.P. Glasser, Ceram. Int. 30 (2004) 875–882.
[2] K. Hirota, G. Komatsu, M. Yamashita, H. Takemura, O. Yamaguchi, Mater. Res. Bull. 27 (1992) 823–830.
[3] Y.T. Yeom, S.H. Choh, M.L. Du, M.S. Jang, Phys. Rev. B 53 (1996) 3415–3421.
[4] D.N. Ke, T.Y. Peng, L. Ma, P. Cai, P. Jiang, Appl. Catal. A: Gen. 350 (2008) 111–117.
[5] F. Rullens, A. Laschewsky, M. Devillers, Chem. Mater. 18 (2006) 771–777.
[6] A. Kudo, K. Omori, H. Kato, J. Am. Chem. Soc. 121 (1999) 11459–11467.
[7] A. Kudo, K. Ueda, H. Kato, I. Mikami, Catal. Lett. 53 (1998) 229–230.
[8] S. Tokunaga, H. Kato, A. Kudo, Chem. Mater. 13 (2001) 4624–4628.
[9] S. Kohtani, M. Koshiko, A. Kudo, K. Tokumura, Y. Ishigaki, A. Toriba, K. Hayakawa, R. Nakagaki, Appl. Catal. B: Environ 46 (2003) 573–586.
[10] L. Zhang, D.R. Chen, X.L. Jiao, J. Phys. Chem. B 110 (2006) 2668–2673.
[11] A. Walsh, Y.F. Yan, M.N. Huda, M.M. Al-Jassim, S.H. Wei, Chem. Mater. 21 (2009) 547–551.
[12] R.S. Roth, J.L. Waring, Am. Mineral. 48 (1963) 1348–1356.
[13] A.W. Sleight, H.Y. Chen, A. Ferretti, D.E. Cox, Mater. Res. Bull. 14 (1979) 1571–1581.
[14] J.Q. Yu, Y. Zhang, A. Kudo, J. Solid State Chem. 182 (2009) 223–228.
[15] S. Kohtani, S. Makino, A. Kudo, K. Tokumura, Y. Ishigaki, T. Matsunaga, O. Nikaido, K. Hayakawa, R. Nakagaki, Chem. Lett. 31 (2002) 660–661.
[16] S. Kohtani, J. Hiro, N. Yamamoto, A. Kudo, K. Tokumura, R. Nakagaki, Catal. Commun. 6 (2005) 185–189.
[17] X. Zhang, Z.H. Ai, F.L. Jia, L.Z. Zhang, X.X. Fan, Z.G. Zou, Mater. Chem. Phys. 103 (2007) 162–167.
[18] Y. Zhao, Y. Xie, X. Zhu, S. Yan, S.X. Wang, Chem. Eur. J 14 (2008) 1601–1606.
[19] M.C. Neves, T. Trindade, Thin Solid Films 406 (2002) 93–97.
[20] L. Zhang, J. Lin, Z. Chen, Y. Tang, Y. Yu, Appl. Catal. A: Gen. 299 (2006) 292–297.
[21] M. Shang, W.Z. Wang, S.M. Sun, L. Zhou, L. Zhang, J. Phys. Chem. C 112 (2008) 10407–10411.
[22] K. Sayama, A. Nomura, T. Arai, T. Sugita, R. Abe, M. Yanagida, T. Oi, Y. Iwasaki, Y. Abe, H. Sugihara, J. Phys. Chem. B 110 (2006) 11352–11360.
[23] M.L. Guan, D.K. Ma, S.W. Hu, Y.J. Chen, S.M. Huang, Inorg. Chem. 50 (2011) 800–805.
[24] S.M. Sun, W.Z. Wang, L. Zhou, H.L. Xu, Ind. Eng. Chem. Res. 48 (2009) 1735–1739.
[25] L.Q. Jing, X.J. Sun, J. Shang, W.M. Cai, Z.L. Xu, Y.G. Du, H.G. Fu, Sol. Energy Mater. Sol. C 79 (2003) 133–151.
[26] Y.H. Lin, D.J. Wang, Q.D. Zhao, M. Yang, Q.L. Zhang, J. Phys. Chem. B 108 (2004) 3202–3207.
[27] B.F. Xin, L.Q. Jing, Z.Y. Ren, B.Q. Wang, H.G. Fu, J. Phys. Chem. B 109 (2005) 2805–2809.
[28] Q.H. Zhang, L. Gao, J.K. Guo, Appl. Catal. B: Environ. 26 (2000) 207–215.
[29] M. Shang, W.Z. Wang, L. Zhou, S.M. Sun, W.Z. Yin, J. Hazard. Mater. 172 (2009) 338–344.
[30] V. Stavila, R.L. Davidovich, A. Gulea, K.H. Whitmire, Coord. Chem. Rev. 250 (2006) 2782–2810.
[31] A. Fitch, S. Dragan, J. Chem. Educ. 75 (1998) 1018–1021.
[32] K.C. Lanigan, K. Pidsosny, Vib. Spectrosc. 45 (2007) 2–9.
[33] K. Norén, J.S. Loring, J.R. Bargar, P. Persson, J. Phys. Chem. C 113 (2009) 7762–7771.
[34] M.C. Long, W.M. Cai, J. Cai, B.X. Zhou, X.Y. Chai, Y.H. Wu, J. Phys. Chem. B 110 (2006) 20211–20216.